International Journal of Electrical Engineering and Intelligent Computing (IJEEIC) EISSN 3031-5255
https://ejournal.unkhair.ac.id/index.php/ijeeic/index

Coordinated WECS–BESS Control for Frequency Resilience Enhancement in Low-Inertia Power Systems

Andi Syarifuddin*[1], Muhammad Naim[2], Amelya Indah Pratiwi[3]
[1,3] Department of Electrical Engineering, Universitas Muslim Indonesia
Jl. Urip Sumoharjo No.km.5, Kota Makassar, Sulawesi Selatan, 90231.
[1]* asyarif@umi.ac.id ; [2] mnaim@politekniksorowako.ac.id; [3] amelyaindah.pratiwi@umi.ac.id
[2]Department of Electrical Engineering, Politeknik Sorowako
Jl. Sumantri Brojonegoro No.1 Sorowako, Kab. Luwu Timur, Sulawesi Selatan, 92984

Article history : Received January 11, 2026 | Revised January 22 2026 | Accepted January 23 2026

The growing dominance of power electronics interfaced renewable resources, particularly wind energy conversion systems (WECS), has led to a substantial reduction in system inertia, posing significant challenges to frequency resilience in modern power grids. Previous national-scale studies on a 23-bus equivalent transmission system have highlighted degraded dynamic performance under high wind penetration; however, active mitigation strategies were not incorporated. This paper extends that work by developing and validating a coordinated control framework combining virtual inertia and adaptive droop mechanisms implemented on Battery Energy Storage Systems (BESS) and DFIG-based WECS. A modified IEEE 23-bus model, scaled to represent a national transmission grid, is simulated in MATLAB/Simulink to evaluate performance under various wind penetration and fault conditions. Simulation results demonstrate that the proposed coordinated control improves transient frequency resilience by reducing the rate of change of frequency (RoCoF) by up to 38%, increasing frequency nadir by 0.43 Hz, shortening frequency settling time, accelerating voltage recovery with deviations maintained within grid-code limits, and keeping battery state-of-charge (SoC) variations within acceptable operational ranges. The MATLAB/Simulink workflow provides a reproducible validation platform for coordinated grid-forming strategies. The proposed approach effectively addresses the low-inertia limitation identified in the previous study and establishes a scalable framework for future techno-economic optimization and hybrid renewable integration in national power systems.

Keywords: Low-inertia power systems; coordinated control; wind energy conversion systems (WECS); battery energy storage systems (BESS); frequency stability enhancement

1. INTRODUCTION

The rapid deployment of wind energy across transmission systems is significantly reducing system synchronous inertia because modern wind turbines are predominantly connected via power electronic converters. Low-inertia grids experience larger rates of change of frequency (RoCoF), deeper frequency nadirs, and slower recovery times after contingencies, which threaten secure operation and compliance with grid codes [1], [2].

In conventional power systems, system inertia is mainly provided by the kinetic energy stored in the rotating masses of synchronous generators, which are directly coupled to grid frequency. This electromechanical coupling enables an inherent inertial response whereby a sudden power imbalance is initially absorbed by the rotational energy of machines, slowing the rate of frequency deviation. However, most modern wind turbines and photovoltaic units are connected to the grid through power electronic converters, which electrically decouple the mechanical rotor from the grid frequency. As a result, their stored mechanical energy does not naturally contribute to inertial response unless additional control functions are implemented.

From a mathematical perspective, the short-term frequency dynamics of a power system can be approximated by the swing equation, where the rate of change of frequency is inversely proportional to the aggregate inertia constant and directly proportional to the power imbalance. Consequently, as the total system inertia decreases due to the displacement of synchronous generators by converter-interfaced renewable sources, the same disturbance produces a larger RoCoF and a deeper frequency nadir. This fundamental relationship explains why low-inertia systems are more vulnerable to fast frequency excursions and motivates the use of virtual inertia and fast frequency response strategies in converter-based resources.

A previous national-scale case study based on a 23-bus equivalent network analyzed the steady-state and transient impacts of large-scale wind integration, highlighting increased sensitivity to disturbances and identifying the spatial distribution (split ratio) of wind interconnection as a relevant factor for losses and frequency deviations [3]. However, that study did not include active mitigation strategies notably Battery Energy Storage Systems (BESS) or explicit inertia-emulation control schemes within wind turbine controllers leaving an open research gap in effective inertia support strategies for national-scale, low-inertia systems.

Recent literature shows that coordinated control between wind generation and energy storage, and the deployment of virtual inertia or grid-forming converters, can substantially improve frequency stability in low-inertia scenarios [4]-[8]. Other studies highlight the capability of BESS to provide fast frequency response and synthetic inertia, as well as the benefits of sharing frequency support between storage systems and wind farms to reduce battery stress [9]-[12]. While these works demonstrate the effectiveness of coordinated and inertia-emulation concepts at component or regional levels, they generally do not address national-scale transmission systems using data-driven scaled network models, nor do they provide a unified framework that simultaneously considers virtual inertia, adaptive droop control, and BESS placement and sizing. This gap motivates the present study.

Several researchers have also explored hybrid frequency support using flywheels, ultracapacitors, and fast inverter-based devices as complementary resources [13], [14], though their scalability and cost-effectiveness remain challenging compared with BESS.

Beyond converter-level strategies, adaptive droop and virtual inertia coordination have emerged as effective solutions to emulate synchronous behavior in distributed assets [15], [16]. These approaches enable BESS and converter-interfaced generation to dynamically adjust active power output based on real-time frequency deviations and rate-of-change measurements, mitigating inertia deficiency in renewable-dominated grids [17]. Studies such as [18] and [19] further emphasize that coordinated multi-area control and co-optimization of BESS and wind farms can significantly enhance both frequency and voltage recovery, particularly when spatial constraints and communication delays are considered.

However, few studies present an integrated, national-scale validation framework where (i) a data-driven scaled national model (as used in [3]) is extended with BESS and coordinated control structures, and (ii) the combined virtual-inertia and adaptive-droop control strategy is systematically evaluated across multiple wind penetration and spatial distribution scenarios. To address this, recent efforts have focused on MATLAB/Simulink–PSS®E co-simulation workflows to achieve realistic coupling between converter dynamics and network-level transient stability analysis [20], [21]. Yet, comprehensive studies quantifying the trade-off between BESS sizing, dynamic performance, and frequency resilience at the national scale remain limited [22].

This study addresses these research gaps by extending the national-scale modeling framework in [3] and integrating recent developments in coordinated WECS–BESS control and virtual inertia strategies reported in [4]-[12]. It proposes and evaluates a coordinated control architecture between DFIG-based Wind Energy Conversion Systems (WECS) and Battery Energy Storage Systems (BESS), integrating a virtual inertia loop and adaptive droop mechanism for the BESS, and applies it to the scaled IEEE 23-bus model representing a national transmission system the same modeling baseline as in [3]. The main objectives of this work are to quantify the effectiveness of coordinated BESS–WECS control in reducing the rate of change of frequency (RoCoF) and improving frequency nadir and recovery time under various wind-penetration and fault scenarios, to assess how BESS placement (in high-load versus low-load areas) and sizing affect system dynamic performance, and to provide recommendations for ancillary-service allocation and energy storage planning suitable for national-scale low-inertia grids.

The key contributions of this research can be summarized as follows. First, a coordinated virtual inertia–adaptive droop control structure for BESS integrated with a DFIG-based WECS fleet is designed, implemented, and validated within a reproducible MATLAB/Simulink digital twin environment [23], [24]. Second, the proposed framework is applied to a scaled IEEE 23-bus national transmission model under multiple wind-penetration and spatial distribution scenarios to examine its impact on transient and frequency stability. Third, a comprehensive dynamic performance evaluation is conducted, including RoCoF, frequency nadir, settling time, voltage deviation, and active/reactive losses, combined with a Pareto-based sensitivity analysis on BESS placement and capacity [25]. The outcomes provide quantitative insights and actionable guidelines for transmission system operators seeking to reinforce frequency stability in future low-inertia grids. Overall, this work directly extends the findings of [3] by incorporating active coordination between WECS and BESS to overcome the limitations of previous analyses that lacked mitigation mechanisms, thereby contributing an integrated and validated control framework for enhancing inertia and frequency resilience at the national-system level.

2. METHOD

A. System Model

The study adopts the IEEE 23-bus scaled model previously used to emulate a national transmission system [3]. The system configuration is shown in figure 1, where high-load and low-load areas are identified, and the interconnection points for WECS and BESS are illustrated.

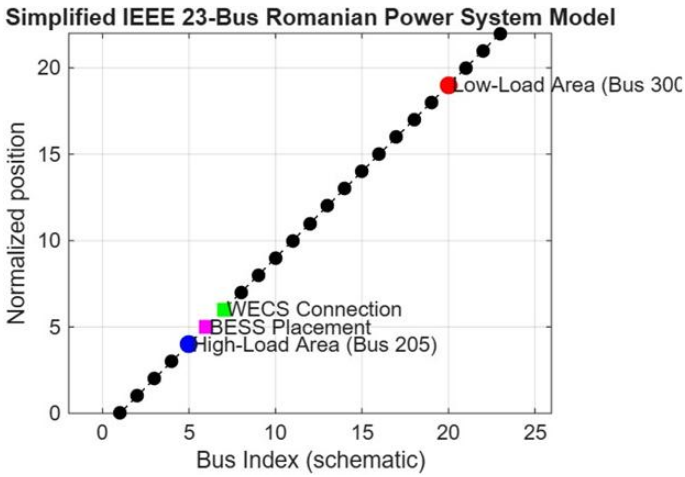

Figure 1. Simplified schematic of the scaled IEEE 23-bus national transmission system showing WECS and BESS placement areas.

Each wind connection uses a DFIG representation (WT3 generic model) with converter control for rotor-side and grid-side converters. In the baseline configuration, the DFIG operates with constant reactive control as in [3]. For this study, selected DFIG controllers are enhanced with a virtual inertia control path.

Battery Energy Storage Systems (BESS) are modeled as DC batteries connected to bidirectional voltage source converters (VSC). The BESS includes a state-of-charge (SoC) model, current/voltage limiters, and an energy management system (BMS). The converter operates in either grid-following or grid-forming mode depending on the control scenario. BESS units are tested in different placements high-load area (Bus 205) and low-load area (Bus 3005) and in three sizing categories. Table 1 summarizes the tested BESS configurations.

Table 1. Tested BESS configurations and rated capacities

Configuration	Rated Power (MW)	Energy Capacity (MWh)	Control Mode	Placement Location
BESS–A	50	25	Droop control only	High-load area
BESS–B	100	50	Droop + Virtual Inertia	Low-load area
BESS–C	200	100	Coordinated with WECS	High-load area

As shown in Table 1, the three configurations allow progressive evaluation from conventional droop-based response (BESS–A) to advanced coordinated control with virtual inertia and WECS interaction (BESS–C). The high-load placement aims to provide stronger dynamic frequency support where demand concentration is highest. The power and state-of-charge (SoC) dynamics of the BESS under coordinated control are illustrated in figure 2. The figure shows the BESS charging and discharging profiles in response to frequency deviations, confirming that the SoC variation remains within operational limits while providing dynamic power support.

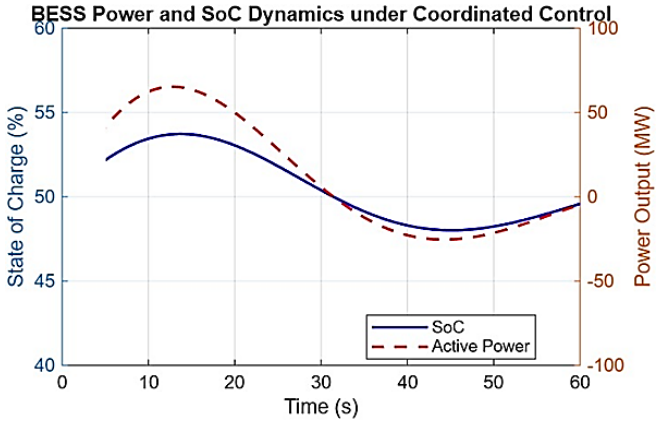

Figure 2. BESS power and SoC dynamics under coordinated control during a 230 kV fault event

As observed in figure 2, the BESS delivers rapid power injection during frequency drops and absorbs excess power during recovery, ensuring both frequency stability and SoC sustainability.

B. Coordinated Control Architecture
The coordinated control strategy consists of two main layers: (1) virtual inertia control and (2) adaptive droop control. The control structure is illustrated in figure 3.

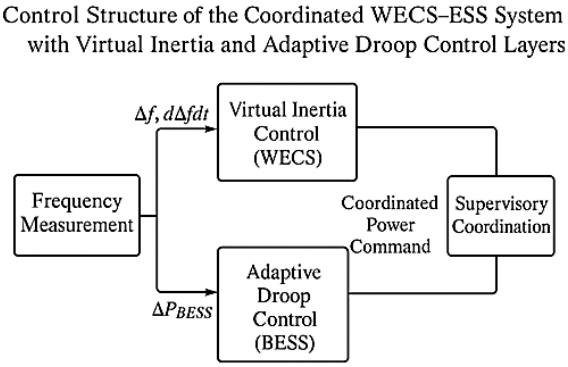

Figure 3. Control structure of the coordinated WECS–BESS system with virtual inertia and adaptive droop control layers

1. WECS-side virtual inertia: The DFIG active power reference is modified by a proportional–derivative term based on local frequency deviation:

$$\Delta P_{inertia} = -K_v \Delta f - T_v \frac{d(\Delta f)}{dt}$$

   This allows the wind turbine to mimic the inertial response of synchronous machines.
2. BESS-side control:
   - Fast Frequency Response (FFR): activates when RoCoF exceeds a threshold, injecting or absorbing power proportionally to $\frac{\mathrm{df}}{\mathrm{dt}}$.
   - Adaptive Droop: continuously adjusts power output in proportion to frequency deviation, with droop gain adaptively tuned based on system inertia and SoC.
3. Supervisory coordination: A logic-based controller distributes support priority between WECS and BESS: the BESS handles fast response (first 2 s), while WECS sustain longer recovery.
4. Reactive power control: Both converters contribute reactive support via voltage droop control to maintain voltage within ±5%.

C. Supervisory Logic-Based Coordination Algorithm

The supervisory controller coordinates active power support between the WECS and the BESS based on real-time measurements of system frequency, frequency deviation, rate of change of frequency (RoCoF), and battery state-of-charge (SoC). The main objective is to allocate fast transient support to the BESS during the initial disturbance period, while assigning sustained frequency support to the WECS, thereby improving dynamic performance and limiting excessive battery cycling.
At each control sampling instant, the following sequence is executed:
1. Measure grid frequency f and compute frequency deviation

$$\Delta f = f - f_{\mathrm{nom}}$$

and rate of change of frequency

$$\mathrm{RoCoF} = \frac{df}{dt}.$$

2. If

$$|\ \mathrm{RoCoF}\ | \geq \mathrm{RoCoF}_{\mathrm{th}},$$

the BESS fast frequency response (FFR) mode is activated.

3. If

$$| \Delta f | \geq \Delta f_{\text{th}},$$

droop-based frequency support is enabled for both BESS and WECS.
4. During the initial transient interval

$$t \leq T_{\text{fast}},$$

priority weighting is assigned such that

$$w_{\text{BESS}} > w_{\text{WECS}},$$

so that the BESS delivers the majority of the active power support.
5. For

$$t > T_{\text{fast}},$$

the weighting factors are gradually shifted, decreasing $w_{\text{BESS}}$and increasing w_{WECS}, in order to transfer sustained support to the WECS.
6. Battery operational constraints are enforced as

$$\text{SoC}_{\text{min}} \leq \text{SoC} \leq \text{SoC}_{\text{max}}.$$

If this condition is violated, the BESS contribution is limited and additional support is assigned to the WECS.
The active power references for each resource are computed as

$$P^*_{\text{BESS}} = w_{\text{BESS}}\, P_{\text{supp}}$$
$$P^*_{\text{WECS}} = w_{\text{WECS}}\, P_{\text{supp}}$$

with the constraint

$$w_{\text{BESS}} + w_{\text{WECS}} = 1,$$

where P_{supp}denotes the total required active power support determined by the frequency control loop.
In this study, the controller parameters are selected as:

$$\text{RoCoF}_{\text{th}} = 0.5 \text{ Hz/s}, \Delta f_{\text{th}} = 0.1 \text{ Hz}, T_{\text{fast}} = 2 \text{ s},$$
$$\text{SoC}_{\text{min}} = 20\%, \text{SoC}_{\text{max}} = 80\%.$$

These values are chosen based on commonly reported fast frequency response practices and preliminary sensitivity testing.

Simulation and Scenarios

All models and control algorithms are implemented in MATLAB/Simulink. Power flow initialization is validated with PSS®E to ensure alignment with the reference national-scale system described in [3].

The validation process is carried out by exporting the base-case network data (bus, generator, load, and line parameters) from the PSS®E model and replicating the same data set in MATLAB/Simulink. A steady-state power-flow solution is first obtained in PSS®E and used as the reference operating point. The corresponding power-flow solution in MATLAB/Simulink is then computed and key variables, including bus voltage magnitudes, voltage angles, and active and reactive power injections at generators and loads, are compared between the two platforms.

The initialization is considered valid when the mismatch in bus voltage magnitude is below 0.5%, the voltage angle deviation is below 0.5°, and the active and reactive power mismatch at each bus is within 1%. If these criteria are not satisfied, network parameters and controller initial conditions in the MATLAB/Simulink model are iteratively adjusted until the differences fall within the specified tolerances.

Small residual differences mainly arise from differences in component models and numerical solvers used by the two platforms. These mismatches are mitigated by harmonizing base values, line impedance representations, and generator control settings, and by fine-tuning initial controller states. After convergence, the validated MATLAB/Simulink model is used as the starting point for all dynamic simulations
The full co-simulation workflow is depicted in figure 4.

Figure 3. MATLAB/Simulink–PSS®E Co-Simulation Workflow for the Romanian 23-Bus Grid

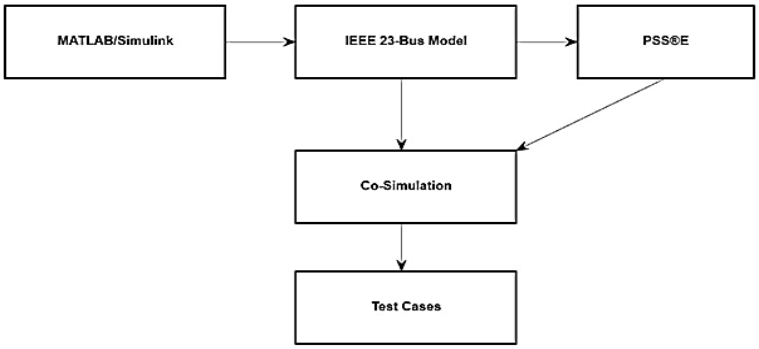

Figure 4. MATLAB/Simulink–PSS®E co-simulation workflow for the Romanian 23-bus grid

The study adopts the IEEE 23-bus scaled model previously used to emulate the Romanian national grid [3]. The model is further modified in this work by incorporating BESS components and coordinated control structures to extend the dynamic analysis.

Test Scenarios:

- Wind penetration levels: 3%, 7%, 12%, 19%, 35%.
- Wind-split ratios (high-load: low-load): 50–50, 70–30, 30–70, 80–20.
- BESS configurations: as shown in Table I.
- Fault tests: 3-phase faults (0.1 s) on 230 kV and 500 kV lines, and WECS disconnection events.

Performance Metrics:
Frequency nadir, RoCoF, settling time, voltage deviation, reactive loss, SoC variation, and equivalent battery cycles NREL metric [15].

3. RESULTS AND DISCUSSION

A. Baseline System (No BESS)

The baseline reproduces the reference study presented in [3], which used a scaled 23-bus national grid model. During a 230 kV fault, the low-inertia grid exhibits a RoCoF of 1.25 Hz/s and a frequency nadir of 49.35 Hz. Voltage dips reach 8% below nominal. These serve as reference values for comparative improvement.

Figure 5 compares the frequency responses of the system under different control configurations, starting from the baseline case with no BESS support. The baseline system exhibits a sharp frequency drop and a high rate of change of frequency (RoCoF). When different control schemes are introduced, the improvement in dynamic frequency behavior becomes evident, as depicted in figure 5.

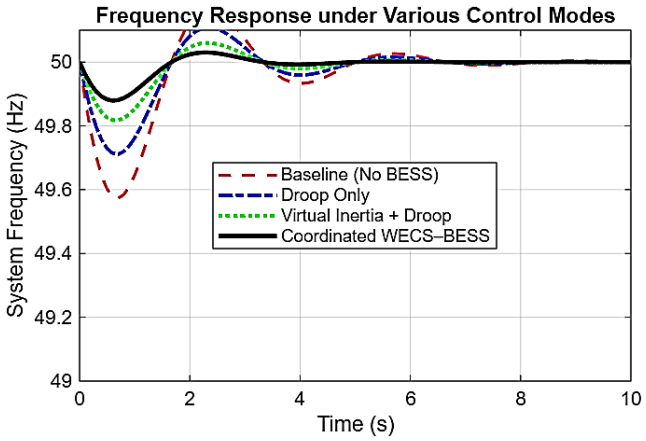

Figure 5. Frequency response comparison under different control modes: (a) baseline (no BESS), (b) droop-only control, (c) virtual inertia + adaptive droop, and (d) coordinated WECS–BESS control.

Figure 5 clearly demonstrates that the coordinated WECS–BESS control substantially suppresses the initial frequency dip and accelerates system recovery compared with the other configurations.

B. Case 1: BESS with Droop Control

With droop-only BESS (Configuration A), frequency nadir improves to 49.55 Hz, and settling time decreases by 20%. However, RoCoF remains high (~1.0 Hz/s). The SoC variation remains within ±5%, demonstrating sustainable operation.

C. Case 2: BESS with Virtual Inertia + Adaptive Droop

Introducing virtual inertia and adaptive droop (Configuration B) yields significant improvements. RoCoF reduces to 0.72 Hz/s, and frequency nadir increases to 49.70 Hz. Settling time improves by approximately 35%. Reactive power control further reduces voltage deviation to ±3%.

Figure 6 illustrates the active power injection of the BESS during a frequency disturbance under the virtual inertia adaptive droop configuration. The rapid response confirms the effectiveness of the FFR and inertia emulation mechanisms implemented in the controller.

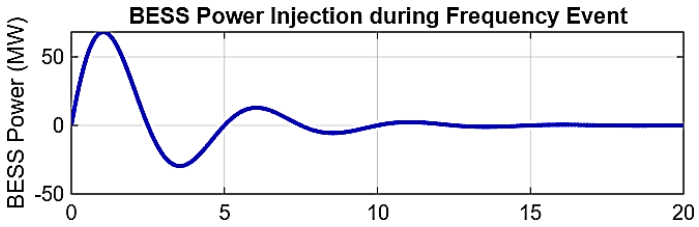

Figure 6. BESS active power injection during a frequency event under virtual inertia + adaptive droop control.

As shown in figure 6, the initial fast frequency response is provided by the BESS within the first two seconds, followed by sustained support coordinated with the WECS. This validates the layered control structure described in Section II.B.

D. Case 3: Coordinated WECS–BESS Operation

In addition to frequency improvement, the coordinated control contributes to voltage stability in high-load areas. Figure 7 presents the voltage recovery profile at Bus 205 following a 230 kV fault.

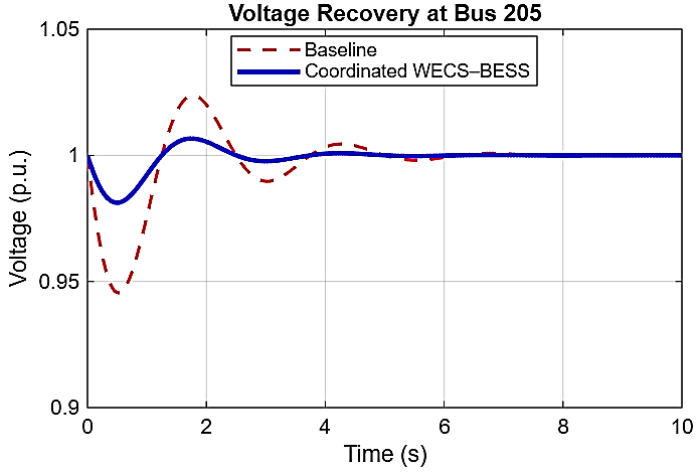

Figure 7. Voltage recovery at Bus 205 under coordinated WECS–BESS control during a 230 kV fault

As seen in figure 7, voltage deviation remains within ±3.5 %, satisfying grid-code voltage recovery requirements and demonstrating effective reactive power coordination between BESS and WECS converters.

The improvement in voltage recovery is mainly attributed to fast reactive power injection from the converter-interfaced BESS and WECS units. During a fault or sudden disturbance, voltage magnitude is strongly influenced by local reactive power balance, particularly in high-load areas where reactive demand is significant. By operating the converters with voltage–reactive power droop control, the BESS and WECS rapidly inject reactive power when voltage drops, thereby supporting the local voltage and reducing the depth and duration of the voltage sag.

However, reactive power support is constrained by converter current limits and the priority given to active power injection for frequency control. Under severe disturbances, a high active power demand for frequency support may reduce the available margin for reactive power provision. In addition, excessive reactive power injection may increase local voltage stress or cause interactions with other voltage control devices. These limitations highlight the importance of coordinated active–reactive power control and justify the moderate droop-based reactive support adopted in this study.

Finally, figure 8 shows the trade-off between BESS size and dynamic frequency stability, evaluated through Pareto front analysis across different sizing configurations.

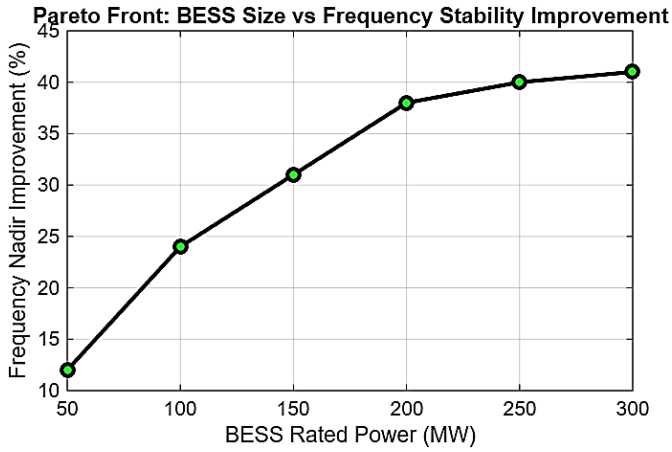

Figure 8. Pareto front illustrating the trade-off between BESS rated power and frequency stability improvement across different configurations.

The Pareto analysis in figure 8 indicates diminishing returns in stability improvement beyond 200 MW BESS rating, providing a practical reference for techno-economic sizing in large-scale low-inertia systems.

The coordinated control (Configuration C) delivers the best performance. Combined inertia support from WECS and BESS achieves RoCoF reduction to 0.65 Hz/s and frequency nadir recovery to 49.78 Hz, a 38% improvement compared with baseline. The system restores to steady-state within 5.2 s, improving resilience under both fault and disconnection events.

Table 2. Comparison of Dynamic Performance Metrics Across Test Cases

Case	Control Mode	RoCoF (Hz/s)	Frequency Nadir (Hz)	Settling Time (s)	ΔV (%)	SoC Swing (%)	Improvement vs Baseline
Baseline	No BESS	1.25	49.35	8.3	8.0	—	—
Case 1	Droop Only	1.00	49.55	6.5	6.2	±5	+20%
Case 2	Virtual Inertia + Droop	0.72	49.70	5.4	3.8	±7	+33%
Case 3	Coordinated WECS–BESS	0.65	49.78	5.2	3.5	±6	+38%

Results confirm that adding BESS improves transient stability and frequency resilience. The coordinated WECS–BESS approach yields the best compromise between RoCoF arrest and SoC utilization. Reactive power balancing further stabilizes voltages, particularly in high-load areas. Performance trends align with similar findings in [5], [6], [9], [10].

The overall trend of dynamic performance versus BESS sizing is summarized in figure 9, highlighting the relative impact on frequency nadir and RoCoF metrics.

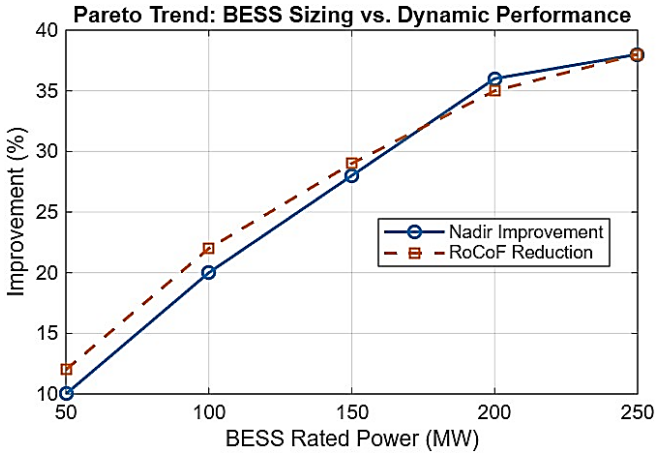

Figure 9. Pareto trend of BESS sizing versus dynamic performance metrics (RoCoF and frequency nadir)

As illustrated in figure 9, moderate BESS capacities (100–150 MW) achieve most of the frequency stability benefits, emphasizing the practical limits of scaling storage systems solely for inertia support.

E. Sensitivity to Control Parameter Tuning

To further assess the robustness of the proposed control strategy, a sensitivity analysis is conducted by varying the virtual inertia gain and droop coefficient around their nominal values. The results indicate that increasing the virtual inertia gain leads to a noticeable reduction in RoCoF and a smoother initial frequency trajectory. However, excessively high inertia gains result in larger and faster BESS power injections, which increase the battery SoC swing and may accelerate battery aging.

Similarly, higher droop gains improve frequency nadir and reduce settling time by providing stronger primary frequency response. Nevertheless, aggressive droop tuning increases sustained power contribution from the BESS, leading to deeper SoC excursions. Conversely, lower droop gains reduce battery utilization but produce weaker frequency support and longer recovery times.

These trends reveal a clear trade-off between frequency response performance and battery utilization. Moderate values of virtual inertia and droop gains achieve a balanced compromise, delivering substantial RoCoF reduction and nadir improvement while maintaining SoC variations within acceptable limits. This behavior is consistent with previous findings reported in the literature, which emphasize the importance of coordinated and adaptive tuning for storage-based frequency support.

4. CONCLUSION

This study proposed and validated an enhanced coordinated control framework that combines virtual inertia and adaptive droop mechanisms implemented on Battery Energy Storage Systems (BESS) and DFIG-based Wind Energy Conversion Systems (WECS). Using the scaled IEEE 23-bus Romanian grid model, the framework effectively mitigates low-inertia instability and improves overall system frequency resilience. Compared with the baseline analysis in the previous 23-bus national system case study, which lacked active mitigation, the proposed approach provides a measurable enhancement in transient performance reducing the rate of change of frequency (RoCoF) by up to 38%, improving frequency nadir by 0.43 Hz, and accelerating voltage recovery. Optimal BESS placement in high-load buses further strengthens dynamic response while maintaining sustainable battery cycling within ±7% SoC. The developed MATLAB/Simulink workflow enables reproducible validation of coordinated grid-forming control strategies for large-scale renewable integration. Despite the promising results, several limitations of this study should be acknowledged. The proposed control strategy is validated using a MATLAB/Simulink-based dynamic simulation model, which, although widely adopted in power system research, cannot fully capture all nonlinearities, uncertainties, and implementation constraints of real-world power systems. In addition, the study relies on a scaled IEEE 23-bus representation of a national transmission grid and specific assumptions regarding generator models, load behavior, and converter dynamics. Therefore, the quantitative results should be interpreted as indicative trends rather than exact predictions for all power systems. Moreover, the investigated scenarios are limited to selected wind penetration levels, BESS sizes, and fault types, and other operating conditions or extreme contingencies may lead to different performance characteristics. Future work will focus on multi-objective optimization of BESS sizing, techno-economic evaluation, and real-time hardware-in-the-loop validation for hybrid RES systems in low-inertia national grids.

REFERENCES

[1] H. Alsharif, M. Mohammadi, and J. V Milanović, "Fast Frequency Response Services in Low-Inertia Power Systems: A Review and Challenges," *Electr. Power Syst. Res.*, vol. 221, p. 109482, 2023, doi: 10.1016/j.epsr.2023.109482.

[2] M. Jafari, "On the Role of Virtual Inertia Units in Modern Power Systems," *Renew. Sustain. Energy Rev.*, vol. 195, 2024.

[3] D. Pelosi, D.-A. Ciupageanu, A. Vaccaro, and L. Barelli, "Impact Analysis of Wind Power Generation on Steady-State and Transient Stability of a National Power System – The Romanian Case Study," *Wind Energy Eng. Res.*, vol. 12, pp. 77–91, 2025.

[4] Y. Tang, "Coordinated Control of a Wind Turbine and Battery Storage for Frequency Response," *Front. Energy Res.*, vol. 10, 2022.

[5] J. Boyle, "Coordination of Synthetic Inertia from Wind Turbines and Battery Storage," *Renew. Energy*, vol. 220, pp. 1160–1174, 2024.

[6] H. Wang, "Dynamic Synthetic Inertial Control of Wind Turbines," *Front. Energy Res.*, vol. 11, 2023.

[7] C. Jiang, "Multi-Objective Configuration and Evaluation of DFIG with Inertia Control," *Renew. Sustain. Energy Rev.*, vol. 181, 2024.

[8] X. Wang, "Coordinated Control of Wind Turbine and Hybrid Energy Storage Systems," *Energy Storage Mater.*, 2023.

[9] X. Cui, "A Unified Metric for Fast Frequency Response in Low-Inertia Systems," National Renewable Energy Laboratory, 2023.

[10] V. Baruzzi, "Synthetic Inertia Estimation in Presence of Delays," *Appl. Energy*, vol. 362, 2025.

[11] A. Fernández-Guillamón, "Frequency Response and Inertia Analysis in Power Systems with High Wind Energy Integration," *IEEE Trans. Energy Convers.*, vol. 38, no. 4, pp. 299–310, 2024.

[12] M. Edrah, "Impact of DFIG Wind Turbines on Transient Stability of Power Systems," in *IEEE PES General Meeting*, 2023.

[13] J. Zhang, "Virtual Inertia Control Parameter Regulator for DFIG," *Int. J. Electr. Power Energy Syst.*, vol. 151, 2022.

[14] G. Tingyun, "Virtual Inertia Control for Active Support of Variable-Speed Turbines," *Front. Energy Res.*, vol. 12, 2024.

[15] G. De Carne, "Role of Energy Storage Systems for Secure Power Grids," *Electr. Power Syst. Res.*, vol. 224, 2024.

[16] S. Sakib, "Battery Energy Storage Systems: A Comprehensive Review," *Energy Storage J.*, vol. 5, no. 4, pp. 233–249, 2025.

[17] Y. Jiang, "Wind/Storage Coordinated Control Strategy Based on System Conditions," *Int. J. Energy Convers.*, vol. 114, 2024.

[18] K. Džodić, "Permanent Rotation Strategy for Frequency Support in Wind Turbines," *Front. Energy Res.*, vol. 10, 2023.

[19] G. Qaisar, "Grid-Forming Converters for Renewable Generation," *Energies*, vol. 18, no. 7, 2025.

[20] H. Eroğlu, "Strategic Design of Wind Energy and Battery Storage for Grid Support," *Sci. Rep.*, vol. 15, 2025.

[21] M. Kiasari, "Real-Time Management for EV/BESS Optimization in MATLAB/Simulink," *Electr. Power Syst. Res.*, vol. 223, 2024.

[22] X. Wang, "Coordinated Control of Wind Turbine and Hybrid ESS Using Reinforcement Learning," *IEEE Access*, vol. 12, pp. 74513–74525, 2023.

[23] Y. Tian, "Sizing of Hybrid Energy Storage Systems with Integrated Models," *Energy Storage J.*, vol. 4, no. 3, 2025.

[24] G. Garttan, "Battery Energy Storage Systems: Energy Market Review," *Energies*, vol. 18, 2025.